Nonlinear Incompressible Finite Element for Simulating Loading of Cardiac Tissue—Part II: Three Dimensional Formulation for Thick Ventricular Wall Segments

A. Horowitz[1]
Department of Biomedical Engineering.

I. Sheinman
Department of Civil Engineering.

Y. Lanir
Department of Biomedical Engineering.

Technion—Israel Institute of Technology, Haifa 32000, Israel

A three dimensional incompressible and geometrically as well as materially nonlinear finite element is formulated for future implementation in models of cardiac mechanics. The stress-strain relations in the finite element are derived from a recently proposed constitutive law which is based on the histological composition of the myocardium. The finite element is formulated for large deformations and considers incompressibility by introducing the hydrostatic pressure as an additional variable. The results of passive loading cases simulated by this element allow to analyze the mechanical properties of ventricular wall segments, the main of which are that the circumferential direction is stiffer than the longitudinal one, that its shear stiffness is considerably lower than its tensile and compressive stiffness, and that, due to its mechanically prominent role, the collagenous matrix may affect the myocardial perfusion.

1 Introduction

In Part I of this article [1], a two dimensional finite element (FE) has been proposed for the simulation of loading of thin myocardial strips. Though providing insight into the mechanical behaviour of the tissue, that element cannot serve for the assembly of models for simulating the mechanics of the thick walled left ventricle (LV), which requires the derivation of fully three dimensional ones.

The present three dimensional FE incorporates both the anisotropy and the material nonlinearity of the myocardium by employing a recently formulated structural constitutive law [2], which is based on the histological composition of the tissue. It utilizes a large deformations total Lagrangian approach together with incompressibility, which requires to consider the hydrostatic pressure (HP) as a fourth nodal variable, in addition to the three displacement components. Unlike in the case of infinitesimal deformations, incompressibility cannot be accounted for by equating Poisson's ratio to 0.5 [3].

Following a preliminary verification, the FE serves for the simulation of several passive loading cases. By performing numerous loading combinations, a large range of mechanical responses is obtained and is analyzed so as to infer the properties of the ventricular wall.

2 Derivation of the Element Equation of Motion

The derivation of the element equation of motion is based on a variational approach, originating from the requirement of minimum potential energy [4, 5]. The total potential energy of the element is given by:

$$\Pi = U + V \tag{1}$$

where U is the strain energy stored in the element and V is the work performed on it by external loads.

Bearing in mind that the myocardium is treated as a hyperelastic material [2], a strain energy function, $W_{(e)}$, from which the stresses are derived, may be defined. Due to the incompressibility constraint, expressed by setting the value of the third invariant of Green's deformation tensor, I_3, equal to unity [4], this function has to be augmented by an additional term:

$$W = W_{(e)} + P(I_3 - 1) \tag{2}$$

where P is a Lagrange multiplier, physically interpreted as the HP in the element. Thus, the strain energy of the element is given by:

$$\Pi(\epsilon_{ij}, P) = \int_{0_v} [W_{(e)} + P(I_3 - 1)]\, {}^0dv + V \tag{3}$$

The stationarity of the total potential energy requires that its first variation in respect to both the strains and the HP should vanish:

$$\delta\Pi = \frac{\partial \Pi}{\partial \epsilon_{ij}}\, \delta\epsilon_{ij} + \frac{\partial \Pi}{\partial P}\, \delta P = 0 \tag{4}$$

[1] Presently, Center for Bioengineering, University of Washington, Seattle, Wash. 98195.

Contributed by the Bioengineering Division for publication in the JOURNAL OF BIOMECHANICAL ENGINEERING. Manuscript received by the Bioengineering Division November 9, 1987; revised manuscript received November 30, 1987.

Since this equality has to hold for any variation over ϵ_{ij} and P, which are unrelated, each of the two variations has to vanish separately:

$$\frac{\partial \Pi}{\partial \epsilon_{ij}} = 0 \tag{5}$$

$$\frac{\partial \Pi}{\partial P} = 0 \tag{6}$$

Expression (5) leads to the equation of motion of the element, while expression (6) leads to the incompressibility equation. The derivation of the equation of motion, which may be found in detail in other sources [4, 6], produces the following general expression:

$$\int_{0_v} {}_0^{t+\Delta t}S^{ij}\,\delta\,{}_0^{t+\Delta t}\epsilon_{ij}\;{}^0dv = {}^{t+\Delta t}R \tag{7}$$

where the 2nd Piola-Kirchoff stresses, ${}_0^{t+\Delta t}S^{ij}$, and the Green-Lagrange strains, ${}_0^{t+\Delta t}\epsilon_{ij}$, at time $t + \Delta t$, are referred to the initial configuration, namely, a total Lagrangian approach is employed (the notation is similar to the one in reference [6]). The right-hand side of equation (7) represents the external loads, generally including surface tractions and body forces. Due to the geometric and material nonlinearities, the equation of motion is nonlinear, and is converted to a sequence of linear equations by incremental decomposition. This process is similar to the one performed for the two dimensional FE [1], however, the final form of the resulting equation is different, since the total stresses at time t, derived from the strain energy function (equation (2)), depend also on the HP:

$${}_0^tS^{ij} = \frac{\partial W_{(e)}}{\partial\,{}_0^t\epsilon_{ij}} + {}_0^tP\,\frac{\partial I_3}{\partial\,{}_0^t\epsilon_{ij}} \tag{8}$$

Therefore, to obtain the stress increment, both the strains and the HP have to be incremented:

$${}_0S^{ij} = \frac{\partial\,{}_0^tS^{ij}}{\partial\,{}_0^t\epsilon_{rs}}\;{}_0\epsilon_{rs} + \frac{\partial\,{}_0^tS^{ij}}{\partial\,{}_0^tP}\;{}_0P \tag{9}$$

where ${}_0\epsilon_{rs}$ and ${}_0P$ are the strain and HP increments, respectively. After substituting the total stress given by equation (8), the resulting expression for the incremental stress is:

$${}_0S^{ij} = \left(\frac{\partial^2 W_{(e)}}{\partial\,{}_0^t\epsilon_{rs}\,\partial\,{}_0^t\epsilon_{ij}} + {}_0^tP\,\frac{\partial^2 I_3}{\partial\,{}_0^t\epsilon_{rs}\,\partial\,{}_0^t\epsilon_{ij}}\right){}_0\epsilon_{rs} + \frac{\partial I_3}{\partial\,{}_0^t\epsilon_{ij}}\;{}_0P \tag{10}$$

When equations (8) and (10) are substituted for the total and incremental stresses, respectively, in the incremental equation of motion [6]:

$$\int_{0_v} {}_0S^{ij}\,\delta_0 e_{ij}\,dv + \int_{0_v} {}_0^tS^{ij}\,\delta_0\eta_{ij}\;{}^0dv$$

$$= {}^{t+\Delta t}R - \int_{0_v} {}_0^tS^{ij}\,\delta_0 e_{ij}\;{}^0dv \tag{11}$$

the resulting final form is:

$$\int_{0_v}\left(\frac{\partial^2 W_{(e)}}{\partial\,{}_0^t\epsilon_{rs}\,\partial\,{}_0^t\epsilon_{ij}} + {}_0^tP\,\frac{\partial^2 I_3}{\partial\,{}_0^t\epsilon_{rs}\,\partial\,{}_0^t\epsilon_{ij}}\right){}_0e_{rs}\,\delta_0 e_{ij}\;{}^0dv$$

$$+ \int_{0_v} {}_0P\,\frac{\partial I_3}{\partial\,{}_0^t\epsilon_{ij}}\,\delta_0 e_{ij}\;{}^0dv + \int_{0_v}\left(\frac{\partial W_{(e)}}{\partial\,{}_0^t\epsilon_{ij}} + {}_0^tP\,\frac{\partial I_3}{\partial\,{}_0^t\epsilon_{ij}}\right)\delta_0\eta_{ij}\;{}^0dv$$

$$= {}^{t+\Delta t}R - \int_{0_v}\left(\frac{\partial W_{(e)}}{\partial\,{}_0^t\epsilon_{ij}} + {}_0^tP\,\frac{\partial I_3}{\partial\,{}_0^t\epsilon_{ij}}\right)\delta_0 e_{ij}\;{}^0dv \tag{12}$$

where ${}_0e_{ij}$ and ${}_0\eta_{ij}$ are the linear and nonlinear parts of the strain increment [6]. The components of the three dimensional incremental strain tensor are:

$${}_0e^T = [{}_0e_{11}\;{}_0e_{22}\;{}_0e_{33}\;2_0e_{12}\;2_0e_{13}\;2_0e_{23}] \tag{13}$$

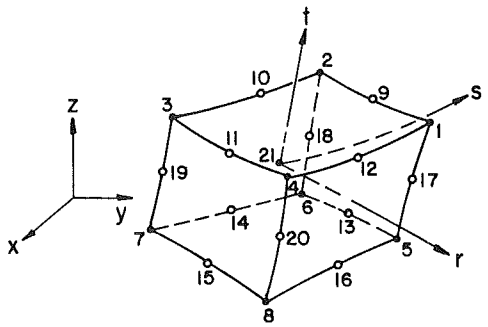

Fig. 1 Outlay of the three dimensional isoparametric 8-21 nodes FE

and the components of the stress tensor at time t are:

$${}_0^tS^T = [{}_0^tS^{11}\;{}_0^tS^{22}\;{}_0^tS^{33}\;{}_0^tS^{12}\;{}_0^tS^{13}\;{}_0^tS^{23}] \tag{14}$$

The nodal variables in the element are the three cartesian components of the displacement and the incremental HP. The present formulation is isoparametric, employing Lagrangian interpolation for both the displacements and the HP. The highest available interpolation order for the displacements is parabolic, resulting in a maximally 21 nodes FE (Fig. 1). As for the HP, it has been argued that its interpolation order should not exceed, or should even be lower than that of the displacements [4]. Consequently, parabolic displacement interpolation calls for linear HP interpolation, and when linear displacement interpolation is employed, the HP should be taken as constant in the element.

The displacements in the element, referred to its cartesian coordinate system, (r, s, t) (see Fig. 1), are given by:

$$u(r,s,t) = \mathbf{H}\,\mathbf{u} \tag{15}$$

where $\mathbf{H}$ is the displacement interpolation functions matrix and $\mathbf{u}$ is the vector of incremental nodal displacements:

$${}_0\mathbf{u}^T = [{}_0u_1^1\;{}_0u_2^1\;{}_0u_3^1\;{}_0u_1^2\;{}_0u_2^2\;{}_0u_3^2\;\cdots\;{}_0u_1^N\;{}_0u_2^N\;{}_0u_3^N] \tag{16}$$

N being the total number of nodes. Similarly, the incremental HP in the element is given by:

$$P(r,s,t) = \mathbf{H}_P\mathbf{P} \tag{17}$$

where $\mathbf{H}_P$ is the HP interpolation functions vector and $\mathbf{P}$ is the vector of incremental nodal HP:

$${}_0\mathbf{P}^T = [{}_0P^1\;{}_0P^2\;{}_0P^3\;\cdots\;{}_0P^M] \tag{18}$$

M being the total number of nodes employed for the HP interpolation, so that $N > M$.

The actual system of equations to be solved for the incremental displacements and for the HP is obtained after expressing the linear and nonlinear parts of the strain increment in equation (12) in terms of the incremental displacements, by employing the appropriate strain-displacement transformation matrices $\mathbf{B}_L$ and $\mathbf{B}_{NL}$ [6], respectively. The ensuing matrix form of the equation of motion is:

$$\left\{\int_{0_v} {}_0^t\mathbf{B}_L^T\left[{}_0\mathbf{C}_{(e)} + {}_0^t\mathbf{H}_P\;{}_0^t\mathbf{P}\,\frac{\partial^2 I_3}{(\partial\,{}_0^t\epsilon)^2}\right]{}_0^t\mathbf{B}_L\;{}^0dv\right.$$

$$\left. + \int_{0_v} {}_0^t\mathbf{B}_{NL}^T\left[{}_0^t\mathbf{S}_{(e)} + {}_0^t\mathbf{H}_P\;{}_0^t\mathbf{P}\,\frac{\partial I_3}{\partial\,{}_0^t\epsilon}\right]{}_0^t\mathbf{B}_{NL}\;{}^0dv\right\}{}_0\mathbf{u}$$

$$+ \left\{\int_{0_v} {}_0^t\mathbf{B}_L\,\frac{\partial I_3}{\partial\,{}_0^t\epsilon}\;{}_0^t\mathbf{H}_P\;{}^0dv\right\}{}_0\mathbf{P}$$

$$= {}^{t+\Delta t}\mathbf{R} - \int_{0_v} {}_0^t\mathbf{B}_L^T\left[{}_0^t\mathbf{S}_{(e)} + {}_0^t\mathbf{H}_P\;{}_0^t\mathbf{P}\,\frac{\partial I_3}{\partial\,{}_0^t\epsilon}\right]{}^0dv \tag{19}$$

where ${}_0^t\mathbf{S}_{(e)}$ and ${}_0\mathbf{C}_{(e)}$ are the elastic part of the stress tensor and of the elastic matrix, given by

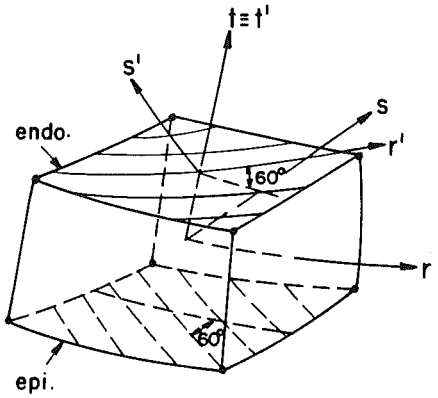

Fig. 2 The global and fiber-attached coordinate systems in a FE which represents an endocardium-to-epicardium LV wall segment

$$ {}^{t}_{0}\mathbf{S}_{(e)} = \frac{\partial W_{(e)}}{\partial {}^{t}_{0}\epsilon} \tag{20} $$

and by:

$$ {}_{0}\mathbf{C}_{(e)} = \frac{\partial^2 W_{(e)}}{(\partial {}^{t}_{0}\epsilon)^2} \tag{21} $$

respectively.

Expression (19) constitutes a system of N equations in N unknown incremental displacements and M unknown incremental HP. The additionally required M equations are obtained by applying the condition of incompressibility.

3 Derivation of the Element Equation of Incompressibility

The equation of incompressibility is obtained by taking the first variation of the total potential energy (equation (3)) in respect to the HP, which, after employing the vector of interpolation functions for the HP, results in:

$$ \int_{0_v} {}^{t}_{0}H_{Pk}(I_3 - 1)\, {}^{0}dv = 0 (k = 1,2, \cdots, M) \tag{22} $$

Similarly to the equation of motion, equation (22) has to be brought to incremental form, which is performed in this case by requiring that the equation still holds when the strains are varied by a small increment:

$$ \int_{0_v} {}^{t}_{0}H_{P_k} \frac{\partial I_3}{\partial {}^{t}_{0}\epsilon_{ij}} \delta_0 \epsilon_{ij}\, {}^{0}dv = 0 \qquad (k = 1,2, \cdots, M) \tag{23} $$

Expression (23) provides the additional M algebraic equations which complete the elemental system of equations. If the HP is taken as constant in the element, expression (23) reduces to a single algebraic equation. The incompressibility equation is obtained in final form by writing the incremental strains in terms of the incremental displacements:

$$ \left[\int_{0_v} {}^{t}_{0}\mathbf{H}_P \frac{\partial I_3}{\partial {}^{t}_{0}\epsilon_{ij}} {}^{t}_{0}\mathbf{B}_L\, {}^{0}dv\right] {}_{0}\mathbf{u} = 0 \tag{24} $$

4 Calculation of the Stress and Elastic Matrix Expressions

The structural constitutive law employed here is based on analysis of the histology of the myocardium and on a general structural theory for fibrous tissues [7]. Its derivation assumes that the main load bearing elements in the tissue are the network of collagen fibers which interconnects the muscle fibers, and the fluid matrix which embeds them. The process of derivation of the stress expressions employs stochastic distribution functions for describing the spatial orientation and the waviness of the collagen fibers, and is similar to the one presented in reference [2]. The available anatomical data [8] indicate that the assumption of linear variation of the muscle fibers angle through the thickness of the ventricular wall, which has been made in reference [2] for thin myocardial strips, is still sufficiently accurate when considering the full wall thickness (notwithstanding, other distribution functions may be equally employed in the present formulation).

The muscle fibers angle is commonly assumed to vary between 60 deg at the endocardium to -60 deg at the epicardium [8]. Therefore, when deriving the stress expressions, the mechanical contribution of the interconnecting collagen fibers (which are given the main mechanical role, [2]) should be summed over this range. This leads to the following expression for the six components of the 2nd Piola-Kirchoff stress tensor:

$$ S^{ij} = s_c \int_{-\pi/3}^{\pi/3} \int_0^{2\pi} \int_0^{\pi} f_c^*(\epsilon_c) R_c(\alpha,\theta,\phi) \frac{\partial \epsilon_c}{\partial \epsilon_{ij}} J\, d\phi\, d\theta\, d\alpha + P \frac{\partial I_3}{\partial \epsilon_{ij}} \tag{25} $$

where s_c is the volumetric fraction of collagen fibers in the myocardium, $R_c(\alpha, \theta, \phi)$ is their spatial distribution function, $f_c^*(\epsilon_c)$ is the uniaxial material law of an ensemble of initially undulated collagen fibers, ϵ_c is their uniaxial strain and J is the Jacobian of transformation from the fiber-attached cartesian coordinates (r', s', t') to the elemental global coordinates (r, s, t) (Fig. 2). These fiber-attached coordinates are rotated in respect to the elemental ones around the t axis, by a varying angle denoted as α.

The members of the 6×6 elastic matrix are obtained by:

$$ C^{ijrs} = \frac{\partial S^{ij}}{\partial \epsilon_{rs}} \tag{26} $$

resulting in:

$$ C^{ijrs} = s_c \int_{-\pi/3}^{\pi/3} \int_0^{2\pi} \int_0^{\pi} \left[\int_0^{\epsilon_c} \frac{D_c(x)}{1+2x}\, dx\right] R_c(\alpha,\theta,\phi) \frac{\partial \epsilon_c}{\partial \epsilon_{ij}} \frac{\partial \epsilon_c}{\partial \epsilon_{rs}} J\, d\alpha\, d\phi\, d\theta - P \frac{\partial^2 I_3}{\partial \epsilon_{rs} \partial \epsilon_{ij}} \tag{27} $$

where $D_c(x)$ is the collagen fibers waviness distribution function [2].

Due to its symmetry, the ensuing elastic matrix contains only 21 separate members.

5 Mode of Solution and Computer Implementation

The complete elemental system of equations for solving the N incremental displacements and the M increments in the HP, which includes the equation of motion (equation (19)) and the equation of incompressibility (equation (24)) is:

$$ \begin{bmatrix} \mathbf{K}_u & \mathbf{K}_P \\ \mathbf{K}_P^T & 0 \end{bmatrix} \begin{bmatrix} \mathbf{u} \\ \mathbf{P} \end{bmatrix} = \begin{bmatrix} \mathbf{F} \\ \mathbf{0} \end{bmatrix} \tag{28} $$

where $\mathbf{K}_u$ is the $N \times N$ matrix of the coefficients of the incremental displacements in equation (19), $\mathbf{K}_P$ is the $N \times M$ matrix of the coefficients of the incremental HP in the same equation, and $\mathbf{F}$ is the vector of nodal forces. The $M \times N$ matrix of the coefficients of the displacements in the equation of incompressibility, is the transposed of $\mathbf{K}_P$. Thus, the assembled stiffness matrix of the element is symmetric, but, due to the inclusion of the constraint of incompressibility, it is not necessarily positive definite [9].

The equations are solved by an incremental-iterative

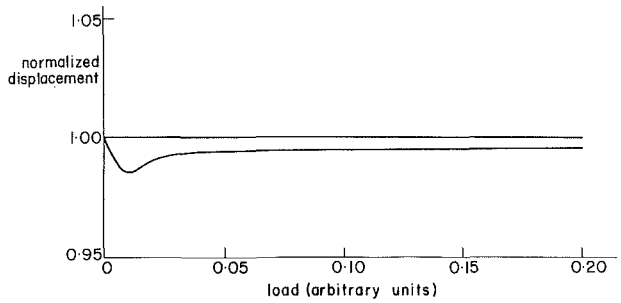

Fig. 3 The normalized difference between the displacements of a two dimensional Mooney-Rivlin FE (straight line) and those of a three dimensional one, under biaxial tension

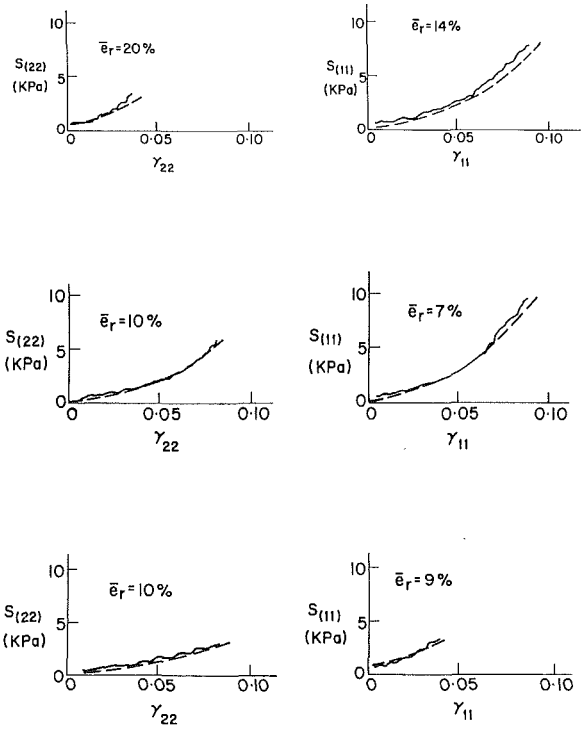

Fig. 4 Comparison between the experimentally measured stresses (continuous line) and those calculated with the three dimensional FE (dashed line) for three loading protocols of the same specimen (right side—fiber direction, left side—cross-fiber direction)

method, similar to the one employed for the two dimensional case [1]. The iterations in each load increment are terminated once the Euclidean norm of the displacements converges, and if the new configuration maintains incompressibility.

The present FE is implemented in a standard structural analysis code [10] by adding subroutines and modifying existing ones at its elemental level. In order to avoid thorough alterations at the global level of the code, which would be required if the HP was to be treated as a fourth nodal variable, the HP is condensed and expressed in terms of the nodal displacements [11]. Since the condensation requires to introduce the kinematic boundary conditions at the elemental level, only a single FE may be presently implemented. For the purposes of this study, which are principally to present the FE formulation and to verify its applicability for simulating passive loading of ventricular wall segments, this option is sufficient.

6 Preliminary Verification

Though similar FE formulations for three dimensional hyperelastic materials, where incompressibility is introduced

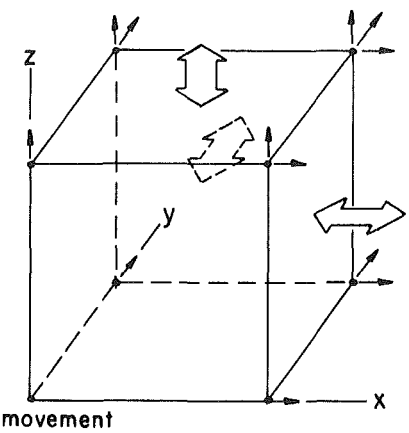

Fig. 5 Kinematic boundary conditions and loading directions for the three dimensional FE

through the HP, have been already performed [4], no computer implementation and numerical results are available in the literature for comparison. Therefore, prior to employing the complete formulation including the structural constitutive law, the FE is verified by implementing a Mooney-Rivlin material model, which is also hyperelastic and incompressible [4], and does appear in standard FE codes (i.e., in [10]) in two dimensional plane-stress elements.

The presently formulated three dimensional FE is compared to the existing two dimensional one by subjecting both of them to identical equi-biaxial tension. When the displacements of the three dimensional FE are compared to those of the two dimensional one, the relative difference between them does not exceed 1.5 percent (Fig. 3). The maximum strains reached in this case are 0.098 in the loading directions and 0.151 in the vertical direction. The incompressibility of the three dimensional FE is found to be preserved within a relative error of 0.13 percent.

Since results of a similar three dimensional FE, containing a structural material law, have not been previously reported, the formulation of the element may be verified only by comparison to the results of mechanical tests. The only available data are those published by Yin et al. [12], in which thin myocardial strips are subjected to tension. In order to allow comparison, the three dimensional FE is subjected to the same three loading protocols as applied on one of the specimens in reference [12] (specimen #2). The variation in the fibers directions through the element is set to be equal to the one in the specimen ($-7.5° \text{ — } +7.5°$), and the material constants appearing in the stress and elastic matrix expressions are ascribed the same values previously estimated for that specimen [2].

The comparison of the calculated stress-strain curves to the measured ones demonstrates an overall very good fit, with average relative errors between 7 to 20 percent at the most (Fig. 4). The errors are similar in magnitude to the ones obtained when the material constants where initially estimated, and reflect the fact that those estimates provide only a close approximation, but not a perfect fit, to the results of the experiments. Therefore, these errors cannot be further diminished.

7 Results

Since the three dimensional FE allows to employ varying fiber directions, it can serve for the examination of the passive mechanical properties of whole segments of the ventricular wall. The fiber direction is assumed to vary between 60 deg at the endocardium to -60 deg at the epicardium [8]. Accordingly, one loading direction corresponds to the circumferential aspect of the LV wall (denoted as the X direc-

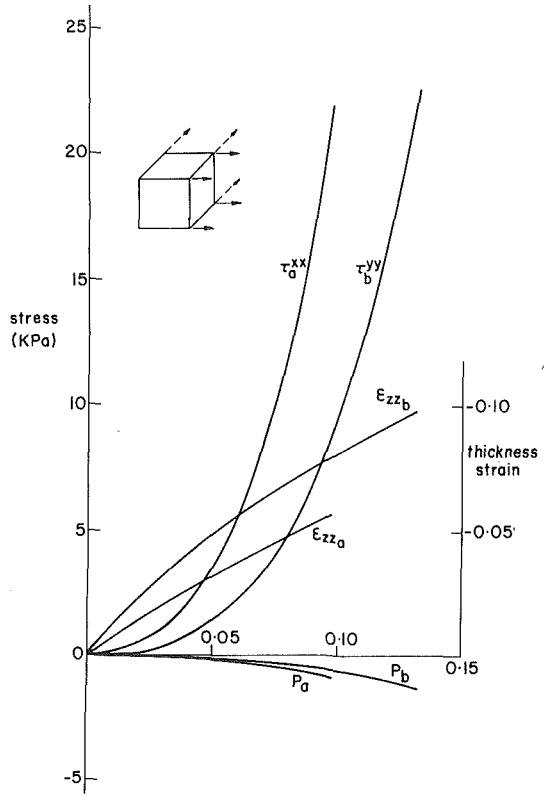

Fig. 6 Stress-strain, hydrostatic pressure (*P*) and thickness strain curves under uniaxial tension in the circumferential (*a*) and in the longitudinal (*b*) directions

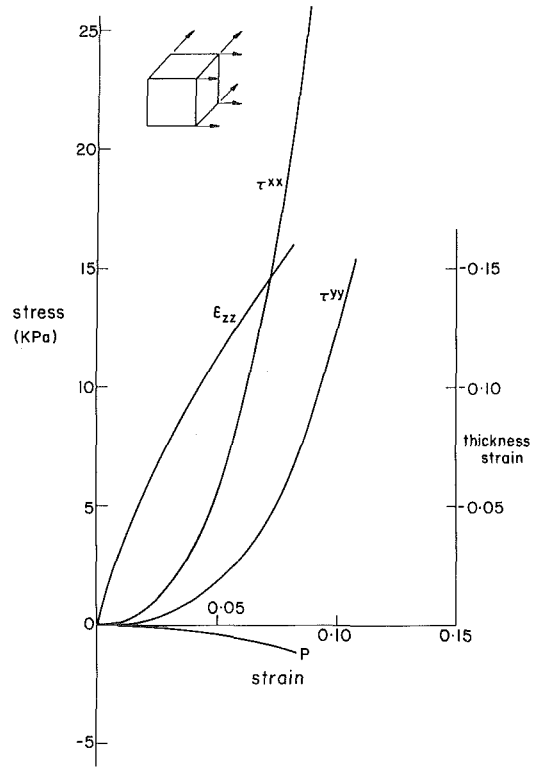

Fig. 7 Stress-strain, hydrostatic pressure (*P*) and thickness strain curves under equibiaxial tension

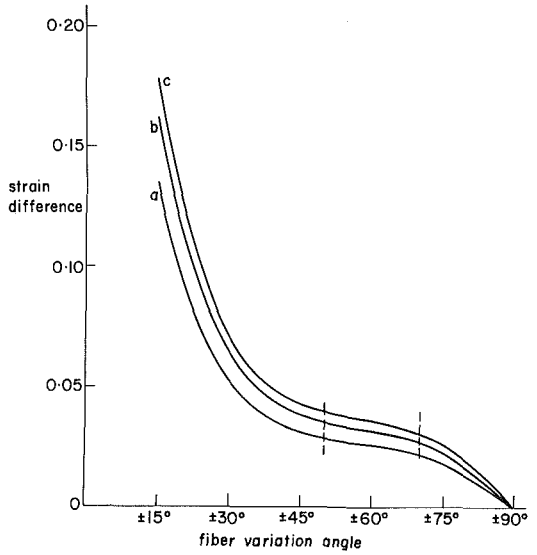

Fig. 8 Strain difference between the circumferential and the longitudinal directions under equibiaxial tension, as a function of fiber distribution range (*a* - for 5 KPa; *b* - for 12.5 KPa; *c* - for 20 KPa).

tion—see Fig. 5), while the other one corresponds to the longitudinal aspect. The present FE may be applied for a wider parametric study than previously performed with the two dimensional FE [1], by adding loading in the vertical direction and by examining the effect of altering the muscle fibers range of distribution.

The loading cases include uniaxial tension in the circumferential and in the longitudinal directions, biaxial tension with several fiber distributions, biaxial tension combined with compression in the vertical direction and simple shear. All the loading cases are performed with a 8-nodes FE (Fig. 5), which is found to provide for these loading modes the same accuracy as a higher order 20-nodes element.

The values employed here for the material constants appearing in the stress and elastic matrix expressions are identical to the ones in the two dimensional FE [1].

The stresses shown in the accompanying figures are Cauchey stress components referred to the present configuration, and are plotted against their corresponding strains (τ^{xx} versus ϵ_{xx}, etc.). The HP is plotted against the thickness strain (ϵ_{zz}).

Uniaxial tension is performed by repeatedly applying twenty increments of 1KPa, in the circumferential (X) and in the longitudinal (Y) directions. The resulting peak strains are 0.098 and 0.133, respectively, indicating that, though the circumferential direction is stiffer than the longitudinal one, the difference is considerably smaller than for parallel fiber arrangement [1]. The HP magnitude reaches only 7 percent of the total tensile stress, denoting that the participation of the fluid matrix in load bearing under tension is small compared to that of the collagen fibers (Fig. 6).

Biaxial tension is carried out by simultaneously applying the same loads as in the former case, in the X as well as in the Y directions. The circumferential direction is found again to be stiffer than the longitudinal one, the peak strains being 0.083 and 0.121, respectively. The HP reaches similar magnitude as in the uniaxial case (Fig. 7).

In order to examine the effect of the fiber directions range of distribution, the biaxial loading case is repeated for fiber distribution ranges of ±15, ±30, ±45 and ±75 deg, in addition to the above ±60 deg range. Comparison between these cases shows that the difference in the stiffness between the circumferential and the longitudinal directions expectedly decreases when the fiber arrangement becomes less unidirectional. When the difference between the tensile strains in the X and in the Y direction for several stress levels (of 5, 12.5 and 20 KPa) is plotted against the fiber distribution range, it is found to decrease relatively slowly between ±50 to ±70 deg

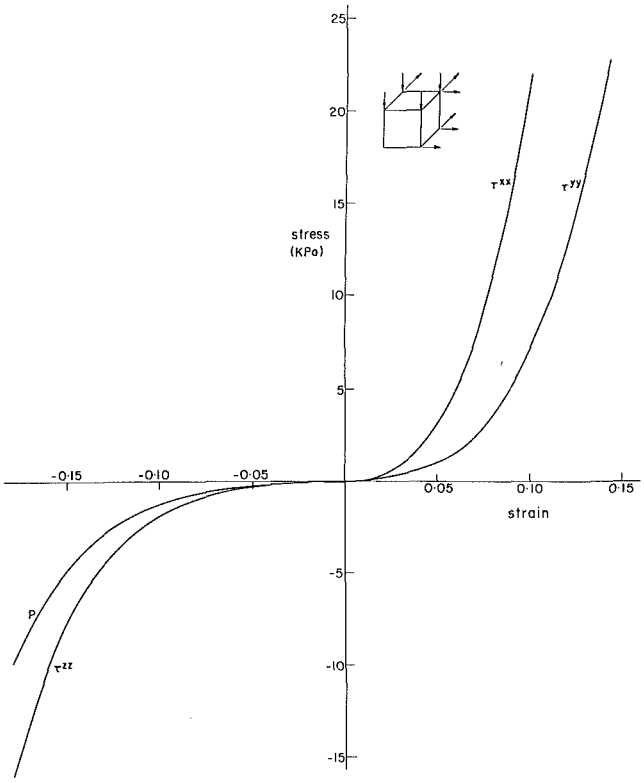

Fig. 9 Stress-strain and hydrostatic pressure (*P*) curves under equibiaxial tension combined with vertical compression

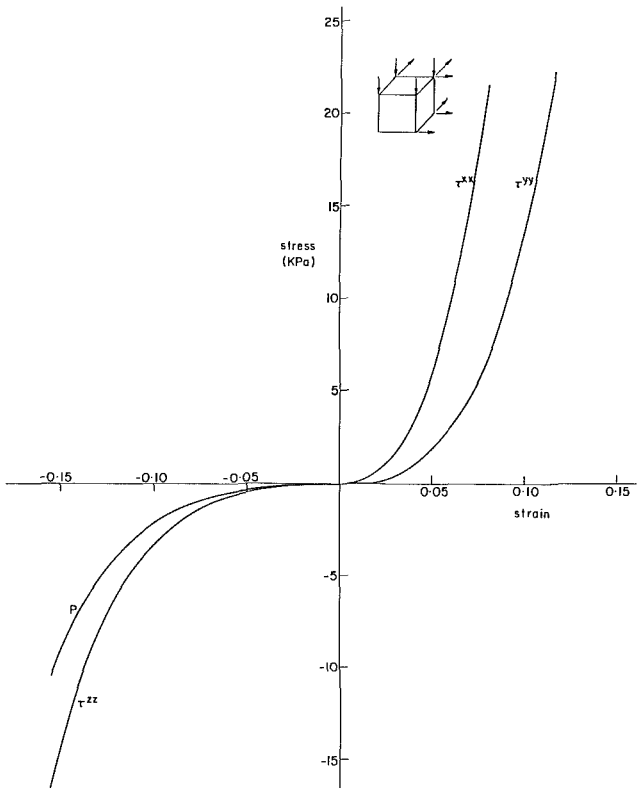

Fig. 10 Stress-strain and hydrostatic pressure (*P*) curves under equibiaxial tension combined with vertical compression, pathological case

(Fig. 8). Since the fiber ranges of distribution in the LV wall are contained between those two values [8], the small variation in the strain difference may indicate that the ratio of the circumferential-to-longitudinal stiffness is relatively uniform over most of the ventricular wall.

Biaxial tension and vertical compression: This case resembles the loading pattern in the LV wall during the heart cycle, when the tensile stresses in the circumferential and longitudinal directions are accompanied by the cavity pressure. The tensile loads are applied in twenty increments of 1KPa in the *X* and *Y* directions, and compression of the same magnitude is applied in the *Z* direction. The tension reaches the same order of magnitude as of the wall stresses calculated by an existing LV FE model [13], and the maximal magnitude of the compression is comparable to the peak intraventricular pressure under normal conditions. The resulting strains in the lateral directions are larger then those in the biaxial tension case, being amplified by the vertical compression (Fig. 9). The HP role is more pronounced relatively to the former cases, being the main component of the *Z* direction normal stress. The compressive stiffness of the tissue turns out to be lower, though not excessively so, than its tensile stiffness.

The present loading case is repeated for a wall segment in which the collagen volumetric fraction is doubled (10 instead of 5 percent), in order to simulate the histological alteration that the myocardium undergoes following infarction [14]. The resulting strains are, expectedly, smaller, and the stresses are considerably higher than those in the intact case (Fig. 10). The peak HP, however, does not significantly exceed the one calculated for the unaffected tissue.

Simple shear is carried out by applying twenty increments of 0.1 KPa tangentially to the four sides of the FE that are parallel to the *Z* axiz. A peak shear strain of 0.109 is obtained in the *X*-*Y* plane, accompanied by a 0.158 thickness strain, as an effect of incompressibility (Fig. 11). The observed shear

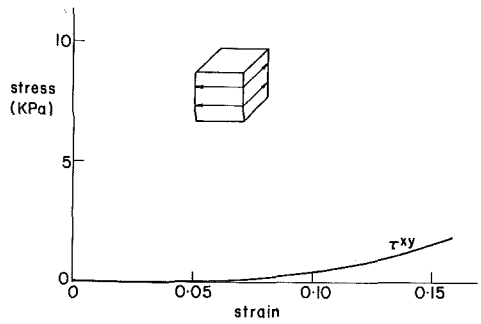

Fig. 11 Stress-strain curve under simple shear

stiffness of the LV wall segment is considerably lower than its stiffness to normal loading, but it is higher than that of a strip which contains only uniformly directed fibers. This is probably because in the present case, a larger portion of the interconnecting collagen fibers are extended due to the wider range of distribution of the muscle fiber directions.

8 Conclusion

Following a previous study, in which a two dimensional FE is formulated and applied for simulating loading of thin myocardial strips [1], a fully three dimensional FE is presently proposed for implementation in LV models. This FE is specifically devised for the myocardium, incorporating its divers mechanical properties: incompressibility, anisotropy and geometric and material nonlinearities. In so doing, it provides a more comprehensive tool for representing cardiac mechanics than formerly available.

By subjecting a single FE to various loading conditions, the mechanical behaviour of a ventricular wall segment is simulated under passive loading. The results of the loading cases demonstrate the different mechanical roles of the net-

work of collagen fibers versus the fluid matrix. While the collagen fibers mainly bear the tensile stresses, the fluid matrix sustains the HP and is the main contributor to the compressive stiffness of the myocardium. These observations are in accordance with the original basic assumptions upon which the presently employed structural material law is based [2]. The evident mechanical importance of the collagenous network in load carrying, and its reported numerous interconnections to the capillaries, imply that it may affect the perfusion regime in the myocardium, as already suggested by another source [15], and as recently analyzed in detail [16]. Consequently, when analyzing the coupling between the stress state in the ventricular wall and the perfusion, the stresses in the solid phase of the tissue should also be considered, in addition to the HP. The HP becomes a prominent factor affecting myocardial perfusion probably when considerable compressive loads are applied on the wall, such as in systole, when the cavity pressure reaches its peak value.

The circumferential stiffness of the LV wall is found to be higher than the longitudinal one. This property, which is a direct outcome of the -60 - $+60$ deg fibers distribution range, may reflect the functional demands imposed on the LV during the cardiac cycle, which probably result in larger loads in the circumferential than in the longitudinal direction. The ± 60 deg fiber distribution through the ventricular wall compensates for the significantly more compliant cross-fiber direction [2], and modifies the circumferential-to-longitudinal stiffness ratio, which would have been much larger for narrower fiber distribution ranges. A similar conclusion is drawn by Yettram et al. [17], which examined the effect of various fiber distributions in a FE model of the LV.

The myocardium is significantly more compliant under shear, compared to its behaviour when subjected to normal loads. Low shear stiffness is also reported in histological studies, where it is attributed to the architecture of the collagen network, which easily permits lateral sliding of fiber bundles [18]. This property may moderate the stresses which develop in the ventricular walls when the heart twists during the cardiac cycle [19].

All the results hitherto reported pertain to single segments of the ventricular wall. Their implications to cardiac mechanics may be extended and confirmed either by carrying further studies with existing LV models, or by implementing the present FE into a complete model of the ventricle.

References

1 Horowitz, A., Sheinman, I., Lanir, Y., Perl, M., and Sideman, S., "Nonlinear Incompressible Finite Element for Simulating Loading of Cardiac Tissue; Part I: Two Dimensional Formulation for Thin Myocardial Strips," ASME JOURNAL OF BIOMECHANICAL ENGINEERING, Vol. 110, 1988, pp. 57-61.

2 Horowitz, A., Lanir, Y., Yin, F. C. P., Sheinman, I., and Strumpf, R. K., "Structural Three Dimensional Constitutive Law for the Passive Myocardium," submitted for publication.

3 Vawter, D. L., "Poisson's Ratio and Incompressibility," ASME JOURNAL OF BIOMECHANICAL ENGINEERING, Vol. 105, 1983, pp. 194-195.

4 Oden, J. T., *Finite Elements of Nonlinear Continua*, McGraw-Hill, New York, 1972.

5 Washizu, K., *Variational Methods in Elasticity and Plasticity*, Pergamon, New York, 1975.

6 Bathe, K. J., *Finite Element Procedures in Engineering Analysis*, Prentice-Hall, Englewood Cliffs, N. J., 1982.

7 Lanir, Y., "Constitutive Equations for Fibrous Connective Tissue," *J. Biomech.*, Vol. 16, 1983, pp. 1-12.

8 Streeter, D. D., and Hanna, T. H., "Engineering Mechanics for Successive States in Canine Left Ventricular Myocardium, II. Fiber Angle and Sarcomere Length," *Circ. Res.*, Vol. 33, 1973, pp. 656-664.

9 Zienkiewicz, O. C., *The Finite Element Method*, McGraw-Hill, New York, 1977.

10 COSMOS7, User's Manual, COSMOS User's Group, S.R.A.C., Santa Monica, Calif., 1984.

11 Horowitz, A., "A Improved Material Model for the Myocardium and its Implementation in the Simulation of the Mechanics of the Left Ventricle," D.Sc Thesis, Technion—Israel Institute of Technology, Haifa, Israel, 1987.

12 Yin, F. C. P., Strumpf, R. K., Chew, P. H., and Zeger, S. L., "Quantification of the Mechanical Properties of Non-contracting Canine Myocardium," *J. Biomech.*, Vol. 20, 1987, pp. 577-589.

13 Perl, M., Horowitz, A., and Sideman, S., "Comprehensive Model for the Simulation of Left Ventricle Mechanics—Part I, Model Description and Simulation Procedure," *Med. Biol. Engng. Comp.*, Vol. 24, 1986, pp. 145-149.

14 Connely, C. M., Vogel, W. M., Wiegner, A. W., Osmers, E. L., Bing, O. H. L., Kloner, R. A., Dunn-Lanchantin, D. M., Franzblau, C., and Apstein, C. S., "Effects of Reperfusion after Coronary Occlusion on Post-Infarction Scar Tissue," *Circ. Res.*, Vol. 57, 1985, pp. 562-577.

15 Borg, T. K., and Caulfield, J. B., "The Collagen Matrix of the Heart," *Fed. Proc.*, Vol. 40, 1981, pp. 2037-2040.

16 Lanir, Y., "The Nature of Interaction between Myocardial Tissue and Intramyocardial Coronary Vessel in the Contracting Heart," *Proc. 4th Henry Goldberg Workshop: Analysis and Simulation of Mechanics, Perfusion and Electrical Performance in Ischaemic Heart Disease*, S. Sideman and R. Beyar, eds., CRC Press, May 1987, Tiberias, Israel, in press.

17 Yettram, A. L., Vinson, C. A., and Gibson, D. G., "Effect of Myocardial Fibre Architecture on the Behaviour of the Human Left Ventricle in Diastole," *J. Biomed. Engng.*, Vol. 5, 1983, pp. 321-328.

18 Caulfield, J. B., and Borg, T. K., "The Collagen Network of the Heart," *Lab. Invest.*, Vol. 40, 1979, pp. 364-372.

19 Ingles, N. B., Daughters, M. S., Stinson, E. B., and Alderman, E. L., "Measurements of Midwall Mycoardial Dynamics in Intact Man by Radiography of Surgically Implanted Markers," *Circulation*, Vol. 52, pp. 859-867.